



HAL
open science

Observation-Based Noise Calibration: An Efficient Dynamics for the Ensemble Kalman Filter

Benjamin Dufée, Etienne Mémin, Dan Crisan

► **To cite this version:**

Benjamin Dufée, Etienne Mémin, Dan Crisan. Observation-Based Noise Calibration: An Efficient Dynamics for the Ensemble Kalman Filter. Stochastic Transport in Upper Ocean Dynamics, 10, Springer International Publishing, pp.43-56, 2023, Mathematics of Planet Earth, 10.1007/978-3-031-18988-3_4 . hal-03910764

HAL Id: hal-03910764

<https://hal.science/hal-03910764v1>

Submitted on 23 Jan 2023

HAL is a multi-disciplinary open access archive for the deposit and dissemination of scientific research documents, whether they are published or not. The documents may come from teaching and research institutions in France or abroad, or from public or private research centers.

L'archive ouverte pluridisciplinaire **HAL**, est destinée au dépôt et à la diffusion de documents scientifiques de niveau recherche, publiés ou non, émanant des établissements d'enseignement et de recherche français ou étrangers, des laboratoires publics ou privés.

Observation-Based Noise Calibration: An Efficient Dynamics for the Ensemble Kalman Filter



Benjamin Dufée, Etienne Mémin, and Dan Crisan

Abstract We investigate the calibration of the stochastic noise in order to guide the realizations towards the observational data used for the assimilation. This is done in the context of the stochastic parametrization under Location Uncertainty (LU) and data assimilation. The new methodology is rigorously justified by the use of the Girsanov theorem, and yields significant improvements in the experiments carried out on the Surface Quasi Geostrophic (SQG) model, when applied to Ensemble Kalman filters. The particular test case studied here shows improvements of the peak MSE from 85% to 93%.

Keywords Stochastic parametrization · Modeling under location uncertainty · noise calibration · Ensemble Kalman filters · Square root filters

1 Introduction

Sequential data assimilation uses observational data to correct a set of realizations given by a numerical model. In the case of both high-dimensional data and model, the data assimilation methodology can be facilitated via a procedure allowing to guide the realizations towards the available observations. This is particularly helpful in high dimensions as it enables the ensemble to focus on a restricted set of the state space. That is what we intend to put forward in this paper. This work relies on a stochastic parametrization of the underlying dynamical system based on the Location Uncertainty (LU) principles, which rely on a decomposition of the Lagrangian velocity into a large-scale smooth component and a random time-uncorrelated component. In this setting, a stochastic transport operator plays the

B. Dufée (✉) · E. Mémin
Inria/Irmar, Fluminance, Campus universitaire de Beaulieu, Rennes Cedex, France
e-mail: benjamin.dufee@inria.fr; etienne.memin@inria.fr

D. Crisan
Department of Mathematics, Imperial College, London, UK
e-mail: d.crisan@imperial.ac.uk

role of the usual material derivative, see [1] for more details. This work aims at adding the feature of a noise specifically calibrated to play a guiding role for the realizations.

In a previous data assimilation study on the Surface Quasi Geostrophic (SQG) model, the stochastic forecast was shown to provide better results than deterministic techniques like variance inflation with perturbation on the initial condition, see [2] for details. The current study is a continuation of [2]. The noise calibration presented here further improves the results presented in [2], particularly when the system starts from poor or badly estimated initial conditions (for instance resulting from initial estimations relying on regularized inverse problems). For such initial conditions, which are generally too smooth and inaccurate, classical ensemble methods are likely to be put in difficulties. In this short paper, we will first briefly recall the principles of Location Uncertainty and how it applies to the SQG model. Then we will detail the procedure leading to the noise calibration, and finally detail and assess the numerical experiments performed.

2 The Stochastic SQG Model Under Location Uncertainty (LU)

The analysis in this paper is carried out on the 2D Surface Quasi-Geostrophic (SQG) model. The SQG equations model an idealized dynamics for surface oceanic currents. It involves many realistic non-linear features such as fronts or strong multiscale eddies (see [3, 4] for details). The deterministic SQG model couples a transport equation of the buoyancy field b , a kinematic condition and a 2D divergence-free constraint:

$$D_t b = 0 ; b = \frac{N_{strat}}{f_0} (-\Delta)^{\frac{1}{2}} \psi ; v = \nabla^\perp \psi, \quad (1)$$

expressed on ψ the stream function and v the velocity, where D_t is the material derivative. The kinematic condition depends on the stratification N_{strat} and the Coriolis frequency f_0 .

The corresponding stochastic dynamics is derived from the Location Uncertainty (LU) principles described in [1]. The full description and numerical analysis of the LU-SQG model can be found in [5, 6]. This stochastic formalism models the impact of the small scales on the flow component that is initially smooth in time. It relies on the decomposition of the Lagrangian velocity of a fluid particle positioned at x_t in a spatial domain $\Omega \subset \mathbb{R}^2$:

$$dx_t = v(x_t, t)dt + \sigma(x_t, t)dB_t, \quad (2)$$

in terms of a resolved component v (referred to as the large-scale component in the following) and σdB_t , an unresolved highly oscillating random component, built

from a (cylindrical) Wiener process B_t (ie a well-defined Brownian motion taking values in a functional space) [7]. The increments of the latter component are time-independent. Due to the lack of smoothness of the solution x_t , we rigorously derive (2) in its integral form.

The random perturbation of velocity is Gaussian and has the following distribution:

$$\sigma dB_t \sim \mathcal{N}(0, Qdt), \quad (3)$$

where Q is the covariance operator. This operator admits an orthonormal eigenfunction basis $\{\phi_n(\cdot, t)\}_{n \in \mathbb{N}}$ with non-negative eigenvalues $(\lambda_n(t))_{n \in \mathbb{N}}$. This generates a convenient spectral definition of the noise as

$$\sigma(x, t)dB_t = \sum_{n \in \mathbb{N}} \sqrt{\lambda_n(t)} \phi_n(x, t) d\beta_t^n, \quad (4)$$

where the β^n are i.i.d standard one dimensional Brownian motions. From Eq. (4), the noise variance tensor a is then defined by

$$a(x, t) = \sum_{n \in \mathbb{N}} \lambda_n(t) \phi_n(x, t) \phi_n(x, t)^T. \quad (5)$$

It can be noticed the variance tensor has the physical dimension of a viscosity (ie m^2/s). Indeed, as σdB_t is a distance, then $a(x, t)dt = E[\sigma dB_t (\sigma dB_t)^T]$ is a squared distance. The procedure used to generate the orthonormal basis functions determines the spatial structure of the noise. The one used in our experiments will be presented later in this section.

While a deterministically transported tracer Θ has zero material derivative: $D_t \Theta = \partial_t \Theta + v \cdot \nabla \Theta = 0$, in the LU framework, a stochastically transported tracer cancels a related stochastic transport operator defined as:

$$\mathbf{D}_t \Theta := d_t \Theta + (v^* dt + \sigma dB_t) \cdot \nabla \Theta - \frac{1}{2} \nabla \cdot (a \nabla \Theta) dt, \quad (6)$$

where

$$d_t \Theta := \Theta(x, t + dt) - \Theta(x, t) \quad (7)$$

is the infinitesimal forward time increment of the tracer. The effective advection velocity is defined by

$$v^* = v - \frac{1}{2} \nabla \cdot a, \quad (8)$$

the term $\sigma dB_t \cdot \nabla \Theta$ is a non-Gaussian multiplicative noise corresponding to the tracer's transport by the small-scale flow, and the last term in (6) is a diffusion term, as the variance tensor a is definite positive. The expression of the stochastic transport operator comes from a generalized Itô formula (Itô-Wentzell formula), see [5] for more details.

The stochastic version of the SQG model is obtained by replacing the material derivative $D_t b$ in Eq. (1) with the stochastic transport operator $\mathbf{D}_t b$:

$$\mathbf{D}_t b = d_t b + (v^* dt + \sigma dB_t) \cdot \nabla b - \frac{1}{2} \nabla \cdot (a \nabla b) dt = 0, \quad (9)$$

and an additional compressibility constraint on the noise:

$$\nabla \cdot \sigma dB_t = 0. \quad (10)$$

In the case of a compressible random field, the modified advection incorporates an additional term in Eq. (8) related to the noise divergence [5]. One essential property of LU (for a divergence-free noise component) is the conservation of energy for the transported random tracer, under the same ideal boundary conditions as in the deterministic case:

$$d \int_{\Omega} \Theta^2(x) dx = 0, \quad (11)$$

and, very importantly, this energy conservation property holds pathwise (i.e for any realization of the Brownian noise), see [5, 8] for details. This property highlights the strong relation between the LU-SQG version and the deterministic one.

Noise Generation The method used to generate the noise in this study relies on a data-driven method called proper orthogonal decomposition (POD) to estimate the empirical orthogonal functions in the spectral representation of Eq. (4). By a slight abuse of notation in the following, this noise will be referred to as POD noise. We give some brief details in what follows.

Considering a series of snapshots of the velocity field, this method consists in the computation of the covariance tensor around the temporal mean of the series of snapshots. Then its eigenvectors and eigenfunctions can be estimated in order to reconstruct the large-scale variability (the first "modes" or eigenfunctions), and the small-scale one (the smaller modes). In practice, this procedure is applied to coarse-grained high-resolution snapshots of deterministic simulations. The latter modes will be the ones on which the noise is decomposed. These modes are divergence-free and stationary by construction, so the global structure of the noise will not vary in time. In case of chaotic geophysical models like this one, we can also use online-computed noises as the one used in our previous work [2] which have much better uncertainty quantification, but are also much more expensive. An extension of this work to this noise is currently at work. We refer to [6] for a precise description of this procedure.

3 Girsanov Theorem and Noise Calibration

3.1 Change of Measure

Ensemble-based sequential data assimilation filters are composed of a forecasting step of the ensemble to provide a sampling of the forecast distribution, and an analysis step correcting the departure from the observations. The purpose of the proposed noise calibration is to modify the forecast distribution, taking into account the upcoming observation, in order to guide the forecast towards it. In the context of transport equations such as in the SQG model, this extra guiding term is an added drift in the noise σdB_t , which was initially built to have zero mean. Allowing σdB_t to have a non-zero mean entails a modification of the transport equation in order to rewrite it in terms of a centered noise. This is called the Girsanov transform, and it consists in a change of underlying measure so that a non-centered noise becomes centered under a new probability measure, up to a drift term accounting for this change of measure. For now, σdB_t is defined on a probability space (Ω, \mathcal{F}, P) and we define $(\mathcal{F}_t)_t$ the filtration adapted to σdB_t .

The Girsanov theorem (see [7] for details) states that if $(Y_t)_{0 \leq t \leq T}$ is a stochastic process such that:

- $(Y_t)_{0 \leq t \leq T}$ is adapted with respect to the Wiener filtration $(\mathcal{F}_t)_{0 \leq t \leq T}$.
- For the current probability measure P , we have, P -almost surely,

$$\int_0^T Y_t^2 dt < \infty.$$

- The process $(Z_t)_{0 \leq t \leq T}$ defined by

$$Z_t = \exp \left(\int_0^t Y_s dB_s - \frac{1}{2} \int_0^t Y_s^2 ds \right) \tag{12}$$

is a \mathcal{F}_t -martingale,

then there exists a probability measure \tilde{P} under which:

- The process $(\tilde{B}_t)_{0 \leq t \leq T}$ defined by

$$\tilde{B}_t = B_t - \int_0^t Y_s ds \tag{13}$$

is a standard cylindrical Wiener process.

- The Radon-Nikodym derivative of \tilde{P} with respect to P is Z_T .

Let us denote by $(\Gamma_t)_{0 \leq t \leq T}$ the drift we intend to add to the noise. With such a change of measure, let us see how Eq. (9) is modified. According to Eq. (13), we have

$$dB_t = d\tilde{B}_t + \Gamma_t dt, \tag{14}$$

so the stochastic transport operator rewrites

$$D_t b = d_t b + (v^* dt + \sigma [d\tilde{B}_t + \Gamma_t dt]) \cdot \nabla b - \frac{1}{2} \nabla \cdot (a \nabla b) dt \quad (15a)$$

$$= d_t b + (v^* dt + v_\Gamma dt + \sigma d\tilde{B}_t) \cdot \nabla b - \frac{1}{2} \nabla \cdot (a \nabla b) dt, \quad (15b)$$

where

$$v_\Gamma = \sum_{k=1}^K \gamma_k \phi_k \quad (16)$$

is the velocity drift entailed by the Girsanov transform and we assume that $\Gamma_t = \Gamma = (\gamma_1, \dots, \gamma_K)$ is constant on a small time step dt , which will be the case for the discretized numerical scheme that we use.

As a result, under the probability measure $\tilde{\mathbb{P}}$, (15) presents the same form as Eq. (9) since \tilde{B} is indeed a centered cylindrical Wiener process under $\tilde{\mathbb{P}}$, but with an added drifted advection velocity.

3.2 Computation of the Girsanov Drift

We now describe how to compute Γ in order to guide the forecast towards the next observation.

Let us start from a given time t_1 where a complete buoyancy and velocity field is available. The next observation $b^{obs}(\cdot, t_2)$ is assumed to be available at time t_2 and L numerical time steps are performed until then ($t_2 - t_1 = L\delta_t$, where δ_t is the time discretization step).

At time t_1 , a rough prediction of the velocity at time t_2 can be estimated with the current velocity (which, more precisely, comes from previous stochastic iterations, but is \mathcal{F}_{t_1} -measurable), namely

$$b^{obs}(x + v(x, t_1)L\delta_t, t_2) := \tilde{b}(x, t_2), \quad (17)$$

that stands for the backward-registered observation with respect to the current deterministic velocity. This way the error made is

$$\Delta_t \tilde{b}(x) = \tilde{b}(x, t_2) - b(x, t_1). \quad (18)$$

So $\tilde{b}(x, t_2)$ is a value taken in a modified observation field, because b^{obs} is advected by the current velocity $v(\cdot, t_1)$. For this reason we consider that the backward-registered observation used for the calibration does not have the same nature as the raw observation used for data assimilation. It constitutes a pseudo-observation,

for which we can consider that the error due to the imprecision of the backward-registration (ensuing in particular from successive bilinear interpolations) is way bigger than the observation noise, and almost uncorrelated to the latter. In the second case, only the raw observation is used for the Kalman filter, corresponding only to the observation noise. The aim is now to calibrate the current velocity by adding a Girsanov drift $v_\Gamma = \sum_{k=1}^K \gamma_k \phi_k$, such that the solution of the following transport equation

$$b \left(x + v(x, t_1)L\delta_t + v_\Gamma L\delta_t + \sum_{k=1}^K (\sqrt{\delta_t}\phi_k)(\sqrt{L\delta_t}\beta_k), t_2 \right) = b(x, t_1). \quad (19)$$

is approximated in a least square sense. In other words, we solve the following minimization problem:

$$\min_{\Gamma} \int_{\Omega} \mathbb{E} \left[b \left(x + v(x, t_1)L\delta_t + v_\Gamma L\delta_t + \sum_{k=1}^K (\sqrt{\delta_t}\phi_k)(\sqrt{L\delta_t}\beta_k), t_2 \right) - b(x, t_1) \right]^2 dx. \quad (20)$$

This can be rewritten as

$$\min_{\Gamma} \int_{\Omega} \left[\Delta_t \tilde{b} + \nabla \tilde{b} \cdot v_\Gamma L\delta_t - \frac{1}{2} \nabla \tilde{b} \cdot \nabla a L\delta_t - \frac{1}{2} \nabla \cdot (a \nabla \tilde{b}) L\delta_t \right]^2 dx.$$

Using the identities

$$\nabla \cdot a = \sum_{k=1}^K (\phi_k \cdot \nabla) \phi_k ; \quad \nabla \cdot (a \nabla b) = \sum_{k=1}^K (\phi_k \cdot \nabla) (\phi_k \cdot \nabla b), \quad (21)$$

we rewrite the minimization problem as

$$\min_{\Gamma} \int_{\Omega} \left[\Delta_t \tilde{b} + \nabla \tilde{b} \cdot \left(\sum_{k=1}^K \gamma_k \phi_k \right) L\delta_t - \frac{1}{2} \sum_{k=1}^K (\nabla \tilde{b} \cdot F_k + G_k(\tilde{b})) L\delta_t \right]^2 dx \quad (22)$$

where

$$F_k = (\phi_k \cdot \nabla) \phi_k ; \quad G_k(\tilde{b}) = (\phi_k \cdot \nabla) (\phi_k \cdot \nabla \tilde{b}).$$

Denoting by J the integrand, we have

$$\frac{\partial J}{\partial \gamma_i} = 2 \int_{\Omega} (\nabla \tilde{b} \cdot \phi_i) L \delta_t \left[\Delta_t \tilde{b} + \nabla \tilde{b} \cdot \left(\sum_{k=1}^K \gamma_k \phi_k \right) L \delta_t - \frac{1}{2} \sum_{k=1}^K (\nabla \tilde{b} \cdot F_k + G_k(\tilde{b})) L \delta_t \right] dx. \quad (23)$$

Finally, we add a regularization term $\alpha \|v_{\Gamma}\|_2^2 = \alpha \sum_{k=1}^K \gamma_k^2 \lambda_k$, where λ_k is the eigenvalue of the Q -eigenfunction ϕ_k in Eq. (22) to ensure the uniqueness of the solution of the proposed minimization problem, where α needs to be tuned properly. As a result, the minimization problem can be written as an inverse problem

$$A\Gamma = c \quad (24)$$

where

$$A_{ik} := 2 \int_{\Omega} (\nabla \tilde{b} \cdot \phi_i) (\nabla \tilde{b} \cdot \phi_k) + 2\alpha \lambda_k \delta_{ik} \quad (25a)$$

$$c_i := \int_{\Omega} (\nabla \tilde{b} \cdot \phi_i) \left[2\Delta_t \tilde{b} - \sum_{k=1}^K (\nabla \tilde{b} \cdot F_k + G_k(\tilde{b})) \right] dx. \quad (25b)$$

The parameter α is a priori fixed in order to control the resulting euclidian norm of v_{Γ} , $\|v_{\Gamma}\|_2$. Large values of α lead to very small corrections (Γ tends to $(0, \dots, 0)$ when α goes to $+\infty$) whereas small values yield very strong and noisy drifts, as we get closer to an ill-posed problem. For now, we use an empirical iterative way to tune α , we increase it until the resulting norm of v_{Γ} is under a given threshold.

4 Experiments

This section details the numerical experiments carried out in this work. The goal is to study the benefits brought by a noise-calibrated forecast in an up-to-date version of a localized ensemble Kalman filter. In particular we wish to observe whether or not the noise calibration brings by itself an efficient and practical improvement of the assimilation step.

Ensemble Kalman filters (see e.g. [9] for details) constitute a well-known family of data assimilation methods. They rely on an ensemble of realizations (called ensemble members) of a dynamical system $(x_n^f)_{n=1, \dots, N}$ coming from the forecast step, and give as an output another set of members $(x_n^a)_{n=1, \dots, N}$. Each posterior ensemble member x_n^a is obtained as a linear combination of the prior ensemble members $(x_n^f)_{n=1, \dots, N}$ in order to minimize the distance between the ensemble and the observation in some sense.

One important assumption of the classical EnKF is to consider that the observation and model noise are uncorrelated. This observation-calibrated forecast could imply that the latter assumption no longer holds. Still, the discussion following Eq. (18) on the observation nature explains why we can consider the uncorrelation between the forecast and observation noise. If this assumption appears to be not valid, we refer to the work made in [10] to rigorously justify the introduction of an observation-dependent forecast. In this work, both Kalman and particle filter equations were rewritten in terms of the conditional expectation with respect to the underlying sequence of current and past observations. The stochastic simulations are run on a double-periodic simulation grid, G_s , of size 64×64 points and of physical size $1000 \text{ km} \times 1000 \text{ km}$, meaning that two neighbor points are approximately 15 km apart. An observation is assumed to be available every day (i.e. every 600 time steps of the dynamics) on a coarser observation grid, G_o , which is a subset of G_s of size 16×16 . It is generated as follows: a trajectory of buoyancy $(z_t)_t$ is run from the deterministic model (PDE) at a very fine resolution grid G_f , of size 512×512 . Then a convolution-decimation procedure D is applied in order to fit to the targeted simulation grid G_s . It consists in the composition of a Gaussian filter and a decimation operator subsampling one pixel out of two. It has to be iterated three times in our case to fit the correct resolution. This is done in order to respect Shannon's theorem and to avoid spectrum folding. A projection operator P is applied from G_s to G_o , and we finally add an observation noise to get the observation

$$b^{obs}(\cdot, t) = P \circ D(z_t) + \eta_t ; \quad \eta_t \sim \mathcal{N}(\mathbf{0}, R) \quad \text{and} \quad R = r^2 I_M, \quad (26)$$

where R is the diagonal observation covariance matrix and M is the number of points on the observation grid.

Numerical Setup The simulations have been performed with a pseudo-spectral code in space (see [6] for details). The time-scheme is a fourth-order Runge-Kutta scheme for the deterministic PDE, and an Euler-Maruyama scheme for the SPDEs. We use a standard hyperviscosity model to dissipate the energy at the resolution cut-off with a hyperviscosity coefficient $\beta = (5 \times 10^{29} \text{ m}^8 \cdot \text{s}^{-1}) M_x^{-8}$, where M_x is the grid resolution [6].

The test case considered in this study is the following: an ensemble of $N = 100$ ensemble members is started from the very same initial condition at day 0, which consists in two cold vortices to the north and two warm vortices to the south. However, the amplitude of the initial vortices is underestimated compared to the initial condition used for the deterministic run (considered as the truth) by 20%, as shown in Fig. 1. We refer to [2] for a mathematical expression of this field.

In this experiment, we study the differences of efficiency of the localized Ensemble Square Root Filter (an up-to-date version of the Ensemble Kalman filter, see for instance [11] for details of the square root filters (ESRF) and [12] for a description of the observation covariance localization procedure) with both noise-calibrated forecast and classical stochastic simulations. We also refer to [13] for the

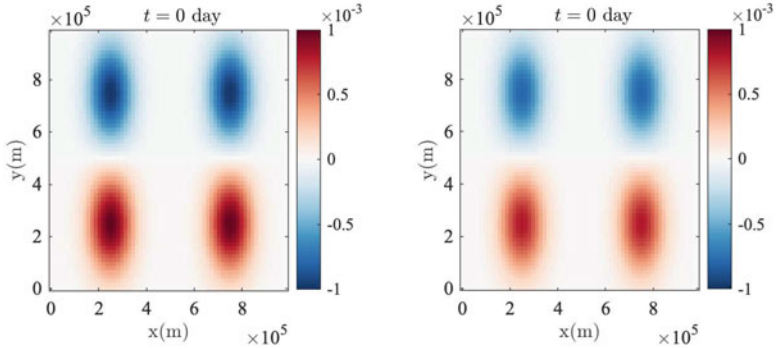


Fig. 1 Initial conditions for the truth (on the left) and for each stochastic run (on the right, common to all ensemble members). We enforce an underestimation of the amplitude of the initial vortices of 20%

extension of the square root filter for additive forecast noise based on covariance transformation, where the advantages of additional model error in the forecast step are shown.

In both cases, starting from the underestimated initial condition, the stochastic dynamics is simulated using the POD noise with $K = 10$ modes. An observation is provided each day (i.e. every 600 time steps of the SPDE), with an observation error covariance set to $r = 10^{-5}$ in (26), which corresponds to a weak (but not negligible, 1% of the maximum amplitude in the initial buoyancy field) noise on the observation. The localization radius is set to l_{obs} here, where $l_{obs} \simeq 60$ km denotes the distance between two neighboring observational sites, as it provided the best results for both cases.

The typical behaviour of the vortices, at least at the beginning of the simulation, is to spin with no translation of the cores. In our case, the true vortices will spin much faster than those in the biased stochastic runs. The goal of calibration is then to speed these vortices up in order to get them closer to the truth.

The forecast is calibrated at each time step of the SPDE, using the upcoming observation to do it. Multiple parameters were tried for the regularization parameter α , or alternatively for the upper bound allowed for the L^2 -norm of the Girsanov drift v_F . Figure 2 compares the MSE along time for all the range of parameters tested here, with also the same experiment without noise calibration. For this latter, the LESRF has a difficult task, as it tries to find linear combinations of the prior ensemble members, which all have an underestimated velocity, to get closer to the observation. This is a general issue for ensemble methods (as well as for particle filters), which are not able and designed to correct the bias if this correction is not made in the forecast. By contrast, the LU calibration offers an additional degree of freedom to guide the ensemble towards the observation. This procedure significantly improves the results in terms of MSE. At day 13, when the MSE is maximal for the usual case, we observe an improvement from 85% to 93% depending on the

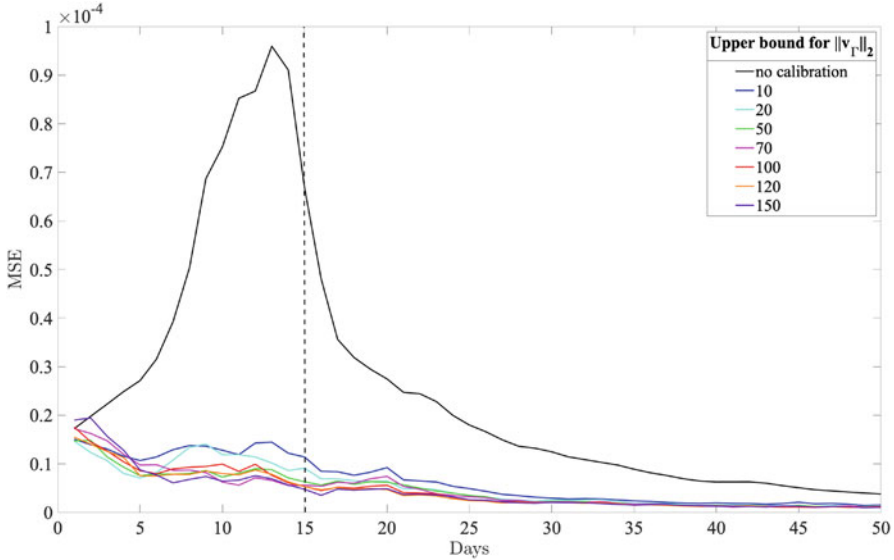


Fig. 2 Comparison of MSE along time between the non calibrated forecast (in black) and all the different parameters tested here for the noise calibration. The snapshots shown in Fig. 3 are taken at day 15 (black dashed line)

parameters tested. The case of the underestimation is an example, but we expect this procedure to be efficient in any situation in which all ensemble members have a similar problem of bias, bad amplitude estimation, artefacts, unsymmetrical features, etc. With a reasonably small ensemble size, which is generally the case in practice, this is likely to occur if the initial conditions have such features.

As explained previously, the regularization term α controls the amplitude of the allowed correction drift. In our experiments, all parameters tested yield significant improvements compared to the classical case, still a good trade-off seems to be found with a control of $\|v_T\|_2$ between 70 and 150. Starting from 150, we observe higher MSE in the very first days, certainly due to a lack of constraint on the inverse problem. In addition to the MSE results, we show in Fig. 3 a more visual example of what calibration does. At day 15, the configuration of the truth is that all four vortices are horizontal. Without calibration (first row), the vortices are slanted because of the initial underestimation of the velocity. The velocity field has not been properly corrected. On the other hand, the LU calibration offers a more reliable prediction, as we recovered the global shape of the vortices, with additional spread around the mean.

Finally, we show in Fig. 4 an insight of how the Girsanov correction v_T behaves in time. As the structure of the noise is stationary, so is the structure of v_T because it relies on the same modes as the noise. What is interesting is the evolution of the amplitude of this field, which decreases in time, meaning that most of the calibration

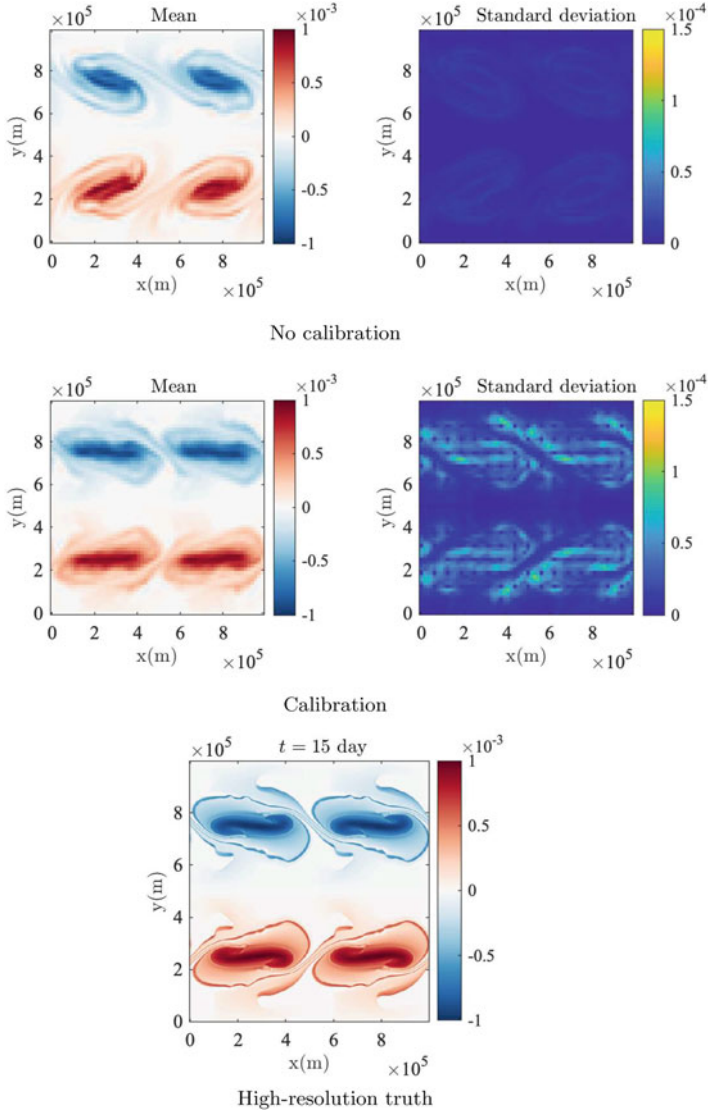


Fig. 3 Comparison between the ensemble mean (left) and the ensemble standard deviation (right) maps, with and without calibration, at day 15 with the high-resolution truth

work is done in the very first days of simulation, and once the forecast manages to get closer to the truth, the need for calibration is less crucial and the Girsanov correction gets weaker.

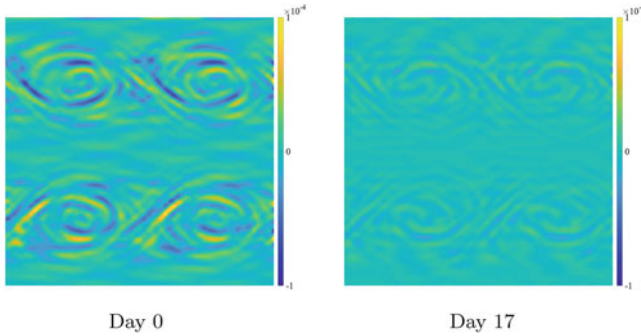


Fig. 4 Vorticity of the Girsanov drift v_T computed for one ensemble member at the first time step after the initial condition (left) and at the first time step after day 17 (right)

5 Conclusion

The findings of this paper show the ability of a data-driven noise calibration procedure to improve significantly the assimilation by EnKF of a system initialized with an underestimated initial condition.

As already mentioned in Sect. 2, we intend to extend this setting to non-stationary noises, as they were shown to be associated to a better quantification of the uncertainty (see [6] for details). Regarding computational effort, the calibration procedure is intrinsically parallelizable ensemble-wise, and the techniques used are close to optical flow estimation procedures, for which efficient solutions exist. The tuning step of α is the more expensive step for now, for which more sophisticated methods could be envisaged.

References

1. E. Mémin. Fluid flow dynamics under location uncertainty. *Geophysical & Astrophysical Fluid Dynamics*, 108(2):119–146, 2014.
2. B. Dufée, E. Mémin and D. Crisan. Stochastic parametrization: an alternative to inflation in EnKF. *Quarterly Journal of the Royal Meteorological Society*, doi:10.1002/qj.4247 2022
3. P. Constantin, Q. Nie, and N. Schörghofer. Front formation in an active scalar equation. *Physical Review E*, 60(3):2858, 1999.
4. G. Lapeyre and P. Klein. Dynamics of the upper oceanic layers in terms of surface quasigeostrophy theory. *Journal of physical oceanography*, 36(2):165–176, 2006.
5. V. Resseguier, E. Mémin, and B. Chapron. Geophysical flows under location uncertainty, Part I: Random transport and general models. *Geophys. & Astro. Fluid Dyn.*, 111(3):149–176, 2017a.
6. V. Resseguier, L. Li, G. Jouan, P. Derian, E. Mémin, and B. Chapron. New trends in ensemble forecast strategy: uncertainty quantification for coarse-grid computational fluid dynamics. *Archives of Computational Methods in Engineering*, pages 1886–1784, 2020a.
7. G. Da Prato and J. Zabczyk. *Stochastic equations in infinite dimensions*. Cambridge University Press, 1992.

8. W. Bauer, P. Chandramouli, B. Chapron, L. Li, and E. Mémin. Deciphering the role of small-scale inhomogeneity on geophysical flow structuration: a stochastic approach. *Journal of Physical Oceanography*, 50(4):983–1003, 2020a.
9. G. Evensen. Sequential data assimilation with a nonlinear quasi-geostrophic model using monte carlo methods to forecast error statistics. *Journal of Geophysical Research: Oceans*, 99(C5):10143–10162, 1994.
10. E. Arnaud, E. Mémin, and B. Cernuschi. Conditional Filters for Image Sequence Based Tracking – Application to Point Tracking *IEEE transactions on image processing : a publication of the IEEE Signal Processing Society*, 14(1):63–79, doi:10.1109/TIP.2004.838707, 2005
11. J.S. Whitaker and T.M. Hamill. Ensemble data assimilation without perturbed observations. *Monthly Weather Review*, 2002.
12. P. Sakov and L. Bertino. Relation between two common localisation methods for the enfk. *Computational Geosciences*, 15(2):225–237, 2011.
13. P.N. Raanes, A. Carrassi, and L. Bertino. Extending the Square Root Method to Account for Additive Forecast Noise in Ensemble Methods *Monthly Weather Review*, 143(10):3857–3873, 2015

Open Access This chapter is licensed under the terms of the Creative Commons Attribution 4.0 International License (<http://creativecommons.org/licenses/by/4.0/>), which permits use, sharing, adaptation, distribution and reproduction in any medium or format, as long as you give appropriate credit to the original author(s) and the source, provide a link to the Creative Commons license and indicate if changes were made.

The images or other third party material in this chapter are included in the chapter's Creative Commons license, unless indicated otherwise in a credit line to the material. If material is not included in the chapter's Creative Commons license and your intended use is not permitted by statutory regulation or exceeds the permitted use, you will need to obtain permission directly from the copyright holder.

